Ferromagnetism and spin transitions in prussian blue: A solid-state hybrid functional study

Derek S. Middlemiss and Chick C. Wilson*
WestCHEM Research School, Department of Chemistry, University of Glasgow, Glasgow, G12 8QQ, United Kingdom
(Received 19 March 2007; revised manuscript received 30 January 2008; published 29 April 2008)

The exchange interactions underlying the weak ferromagnetism of the prototypical mixed valence compound prussian blue (represented by $K^+Fe^{3+}[Fe^{2+}(CN)_6]$) and a Cr^{3+} substituted analog are investigated within a series of solid-state hybrid density functional calculations. Weights of Hartree–Fock (HF) exchange in the range from 30% to 100% are used. The magnetic order in these compounds is shown to be dominated by the coupling of nearest-neighbor high spin (HS) Fe^{3+}-Fe^{3+} and Cr^{3+}-Cr^{3+} pairs, and not by the delocalization of spin along the $\cdots$NC—Fe^{2+}—CN$\cdots$ pathways as previously proposed. The functional containing 35% HF exchange yields an estimated critical temperature for spin ordering and a magnitude for weak Fe^{2+} spin polarization in good agreement with experimental data. The energies of the Fe^{2+} low spin (LS)$\rightarrow$HS ($t_{2g}^6 \rightarrow t_{2g}^4 e_g^2$) and Fe^{3+} HS$\rightarrow$LS ($t_{2g}^3 e_g^2 \rightarrow t_{2g}^5$) excitations are determined and compared with the results obtained previously in a range of Fe^{2+} coordination compounds. It is concluded that the accurate description of these transitions requires the use of a weight of HF exchange below the stable limit of 35% attained in the current study. However, the trends in the present results indicate that the Fe^{3+} HS$\rightarrow$LS excitation is lower in energy than the Fe^{2+} LS$\rightarrow$HS, and also that there is no reasonable prospect of a temperature-induced spin crossover in either compound.

DOI: 10.1103/PhysRevB.77.155129 PACS number(s): 71.70.Gm, 71.15.Mb, 71.70.Ch

I. INTRODUCTION

The analogs of prussian blue (PB) are a fascinating and versatile group of materials that display a wide variety of magnetic properties, including photo-[1] and piezomagnetism,[2] high critical temperatures,[3] and pole inversions.[4] The stoichiometries of these compounds are highly variable, but may be expressed, for the simplest bimetallic systems, in the form M_xA$[$B$(CN^-)_6]_y \cdot n$H$_2$O, where M denotes an alkali or alkaline earth metal cation, and A and B label the nitrogen- and carbon-adjoining transition metal (TM) sublattices, respectively, of the fcc structure. Materials in which multiple species occupy the metal sublattices are also known.[4–6] The diversity in composition aside, a commonality of structure is apparent within these materials, for they all form lattices similar to that of the parent "insoluble" PB compound $Fe^{3+}{}_4[Fe^{2+}(CN)_6]_3 \cdot nH_2$O ($n$=14–16). We note, however, that the charges borne by A and B sublattice ions are often in the reverse order in the analogs.

The magnetic properties of PB itself are of fundamental interest and form the main focus of the current study. A qualitatively correct model of the ground state electronic structure may be obtained by combining the crystal field theory with a knowledge of the properties of the CN^- anion. Thus, the Fe^{2+} ions adopt a low spin (LS) t_{2g}^6 configuration as a consequence of the strong ligand field arising from the adjoining carbon atoms, while the Fe^{3+} ions experience a weaker field and manifest in the high spin (HS) $t_{2g}^3 e_g^2$ configuration. The coupling of the latter moments is consequently likely to be weak, for the exchange interactions must traverse a long pathway comprising two CN^- ligands and a diamagnetic LS Fe^{2+} site, as shown in Fig. 1.

Returning to the PB analogs (PBAs), it is clear that the recent interest in these materials has been largely due to the potential for high critical temperatures in compounds in which both TM sublattices bear magnetic ions.[7,8] The strength of the coupling in these cases arises from the fact that the exchange interactions are conveyed by short bridges consisting of single CN^- ligands. Moreover, the couplings are amenable to simple analyses based on orbital symmetry and overlap, so that the ground state magnetic order of a given PBA can often be predicted directly from a knowledge of the d electron configurations of the constituent TM ions.[3] In contrast, however, our initial survey suggests that the nature of the ordering in PB may be substantially more complex, for it is conceivable that the presence of the LS Fe^{2+} ions on the B sublattice might weaken the ligand-mediated interactions (denoted J_2 in Fig. 1) to the extent that they become comparable with the coupling between nearest-neighbor (nn) HS Fe^{3+} sites (J_1 in Fig. 1). The calculation of the relative strengths of these interactions is the main aim of the current work.

The structure of PB has been determined by the single crystal x-ray diffraction experiments of Buser *et al.*[9,10] Forms of both high and low symmetries were obtained, corresponding to disordered and ordered arrangements, respectively, of $Fe^{2+}(CN)_6$ vacancies and associated water molecules.[9,10]

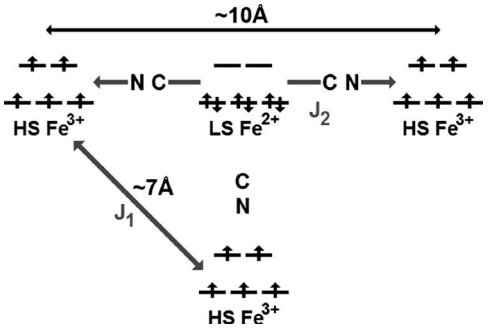

FIG. 1. Nearest-neighbor (J_1) and next-nearest-neighbor (J_2) magnetic interactions, and Fe ion d-electron configurations in FM PB.

Herren *et al.*[11] also reported on a neutron diffraction study of PB lattices at varying degrees of hydration. Dunbar and Heintz[12] provided a summary of the previous structural work within their comprehensive review of the TM cyanides.

Ito *et al.*[13] performed one of the earliest studies of the magnetism in PB, obtaining ferromagnetic order below a critical temperature of 5.6 K. The subsequent neutron diffraction experiment of Day *et al.*[14] confirmed the parallel alignment of the Fe^{3+} moments in the ordered low temperature state and revealed significant spin polarization on the nominally diamagnetic Fe^{2+} ions. Mayoh and Day[15] went on to propose that the ferromagnetism arises from and is stabilized by the mixing of some fraction of the Fe^{2+}-Fe^{3+} intervalence charge transfer excited state into the ground state. We refer to this as the "spin-delocalization" mechanism throughout the present study. The low ordering temperature of PB renders the practical application of the magnetism of this material unlikely. We deem this of little consequence, drawing the motivation for the current work from the historical importance of PB as a prototypical mixed valence system and from the understanding that ions in LS states are a common feature of the technologically relevant photo-and piezomagnetic materials.[3] Examples in the latter context include the pressure-induced linkage isomerism in $K_{0.4}Fe_4[Cr(CN)_6]_{2.8}\cdot 16H_2O$, leading to a Fe^{2+} HS$\rightarrow$LS transition and a strong piezomagnetic effect,[2] and the photomagnetism of $Co^{3+}Fe^{2+}$ PBAs arising out of light-induced $Co^{3+}Fe^{2+}$ (diamagnetic) $\rightarrow Co^{2+}Fe^{3+}$ (magnetic) excitations.[1] The weak ferromagnetism in $Fe^{3+}[Fe^{3+}(CN)_6]\cdot 4H_2O$ is also associated with the presence of LS Fe^{3+} ions.[16]

Prior theoretical studies of PB exist within the literature, but they are less common than those addressing the PBAs.[17–19] We note, in particular, the work of Wojdeł and Bromley,[20,21] which showed that ultrasoft pseudopotentials lack the transferability necessary to accurately represent both Fe^{2+} and Fe^{3+} ions with a single potential. The mixed pseudopotential approach they proposed produces lattice constants and ligand-metal bond lengths in good agreement with experimental values. More recently, the same authors examined the variations in band gap arising from the substitution of a range of alkali metal cations into the PB lattice.[22] Trends in qualitative agreement with experiment were obtained, although the use of a pure density functional approach led to the systematic underestimation of the gap widths. We note, however, that there have been no previous theoretical studies of the magnetism of PB.

We shall establish whether hybrid functionals containing variable amounts of Hartree–Fock (HF) exchange can provide an accurate description of PB and related materials. The main properties of interest are the magnetic coupling constants and associated critical temperatures, and the Fe^{2+} LS($S=0$)$\rightarrow$HS($S=2$) and Fe^{3+} HS($S=\frac{5}{2}$)$\rightarrow$LS($S=\frac{1}{2}$) excitation energies. The magnitudes of the J_1 and J_2 couplings will be examined in detail, given that the previous model of the ferromagnetic state included only the latter contributions.[15] A similar set of properties will be determined for the analogous $Cr^{3+}Fe^{2+}$ compound (denoted "CrPB") on the basis that the differences in orbital occupation and overlap will provide a useful comparison. The structural models and computational methods used are detailed first, followed by the calculated bond lengths, atomic charges, spin moments, and electronic structure. The results relating to the spin transitions and magnetism follow these preliminaries, while the discussion and conclusions place our findings within the context of related studies.

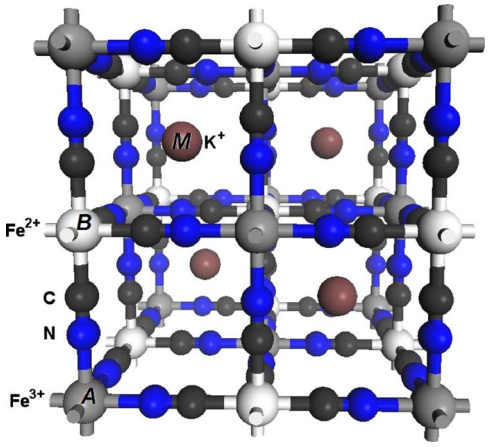

FIG. 2. (Color online) The conventional cell of $KFe^{3+}[Fe^{2+}(CN)_6]$. A, B, and *M* label metal sublattices.

II. STRUCTURES AND COMPUTATIONAL METHODS

The calculations adopt model anhydrous structures of PB and CrPB, in which the TM sublattices are fully occupied. Charge balancing K^+ ions are placed at one-half of the available *M* sublattice sites, yielding lattices of $F\bar{4}3m$ symmetry. The conventional cell of the resulting model for PB is shown in Fig. 2. Save in our use of K^+ rather than Na^+ cations, it is similar to the linear $\cdots Fe^{2+}$—C$\equiv$N—$Fe^{3+}\cdots$ structures used in the previous simulations of PB (Refs. 20–22) and constitutes a close approximation to the structure of "soluble" PB.[12,23] Fixed lattice constants are used throughout, so as to avoid the introduction into the coupling constants of any error due to inaccuracies in the HS ion separations. The value of 10.13 Å obtained from the neutron diffraction study of dehydrated $Fe^{3+}_4[Fe^{2+}(CN)_6]_3$ (Ref. 11) cannot be directly applied in the current calculations for our model structure lacks a comparable distribution of $Fe^{2+}(CN)_6$ vacancies. Instead, we adopt a lattice constant of 10.28 Å derived from representative experimental Fe^{2+}—C, Fe^{3+}—N, and C$\equiv$N bond lengths of 1.94, 2.06, and 1.14 Å, respectively,[11] coinciding with the value proposed by Verdaguer and Girolami.[3] Wojdeł and Bromley[20] adopted identical experimental bond lengths for comparison with their computed structures, save that they use a C$\equiv$N distance of 1.13 Å. Given the lack of a well-defined experimental structure, the sensitivity of the computed exchange interactions to variations in the lattice constant is determined and discussed in Sec. III F. We apply the same fixed cell length to CrPB, with the justification that our main interest is in the gross effects of Cr^{3+} substitution on the magnetism of the lattice. However, the limitations of this methodology are clear, and supplementary studies within fully optimized lattices are intended as part of a wider consideration of the effects of pres-

sure on these compounds. The ferromagnetic (FM) and antiferromagnetic type-I (AF_1) and type-II (AF_2) states are represented within 2 f.u. (30 atom) supercell expansions of the rhombohedral primitive cell. The alignments of the atomic spin moments within these states are detailed in Sec. III F.

The calculations are performed within the CRYSTAL03 code.[24] The crystalline orbitals are expanded in terms of atom-centered basis sets comprising linear combinations of Gaussian functions. The C and N atoms are represented by the valence-reoptimized 6-311G* sets used in our recent study of a $Mn^{2+}Cr^{3+}$ PBA;[25] the Fe^{2+}, Fe^{3+}, and Cr^{3+} ions by 8-6411d41G sets previously optimized for the correct charge state; and K^+ by an optimized 8-6511G set.[26] Hybrid functionals of the form

$$f^{xc} = \frac{100 - F_0}{100}(f^x_{\mathrm{LSDA}} + 0.9\Delta f^x_{\mathrm{B88}}) + \frac{F_0}{100} f^x_{\mathrm{UHF}} + 0.81 f^c_{\mathrm{LYP}} + 0.19 f^c_{\mathrm{VWN}},$$

are applied, where x and c denote exchange and correlation contributions respectively; LSDA, B88, and UHF, the local spin density approximation, Becke-88,[27] and spin-unrestricted HF exchange potentials, respectively; and VWN and LYP, the Vosko–Wilk–Nusair[28] and Lee–Yang–Parr[29] correlation potentials, respectively. The F_0 parameter controlling the HF exchange content of the functionals is varied in the range 30%, 40%,…, 100%. Calculations at lower F_0 values encounter convergence difficulties due to the instability of the wave function and are not pursued further. The F_0=35% functional is included on the basis of a recent study by Feng and Harrison[30], which showed that it provides magnetic coupling constants in good agreement with experiment in a wide variety of TM compounds. The UHF exchange potential ($f^{xc}=f^x_{\mathrm{UHF}}$) is also included as an exemplar of an uncorrelated Hamiltonian.

The positions of the free C and N atoms in the FM ground state are optimized in each Hamiltonian, applying total energy and rms force convergence tolerances of 10^{-7} hartree and 0.0005 hartree $Å^{-1}$, respectively, with the lattice constant fixed as discussed above. The energies of the FM, AF_1, and AF_2 states in each Hamiltonian are subsequently obtained from a series of accurate single point calculations within the appropriate optimized geometry. The low critical temperature of PB leads us to expect that the states will be close in energy, and so we pay particular attention to the convergence of the calculations with respect to the adjustable numerical parameters. Extensive tests spanning the range of F_0 values indicate that a total energy convergence tolerance of 10^{-8} hartree, reciprocal space sampling on an $8\times8\times8$ mesh, and Coulomb and exchange series truncation thresholds of 10^{-9}, 10^{-9}, 10^{-9}, 10^{-9}, and 10^{-18} are sufficiently stringent, where the parameters are as defined in the CRYSTAL03 documentation.[24] We estimate that the uncertainties in the coupling constants due to incomplete convergence range from approximately 6% at F_0=35% to 16% at the UHF level.

TABLE I. The optimized bond lengths, d (Å), in PB for a fixed conventional cell length of 10.28 Å. Experimental values are from the neutron diffraction study (Ref. 11)

F_0	$d(Fe^{HS}—N)$	$d(C\equiv N)$	$d(Fe^{LS}—C)$
30	2.059	1.157	1.924
35	2.056	1.154	1.930
40	2.053	1.151	1.936
50	2.045	1.146	1.948
60	2.038	1.141	1.960
70	2.033	1.137	1.970
80	2.027	1.133	1.980
90	2.023	1.129	1.988
100	2.019	1.126	1.996
UHF	2.018	1.130	1.992
Expt.	2.06	1.14	1.94

III. RESULTS

A. Bond lengths

The bond lengths obtained from the optimizations of PB are presented in Table I. Hamiltonians with high contents of HF exchange produce inaccurate geometries characterized by near equal Fe^{3+}—N and Fe^{2+}—C bond lengths, while the lower F_0 methods yield structures in better agreement with experiment. The discrepancies observed at high F_0 are unlikely to be a manifestation of the difficulties encountered by Wojdeł and Bromley in their pseudopotential-based studies,[20–22] for the present calculations employ basis sets optimized separately for the Fe^{2+} and Fe^{3+} charge states. Given that the Fe^{2+}—C distances vary most markedly across the range of Hamiltonians, we instead suggest that the discrepancies are due to the overestimation of the LS Fe^{2+} ionic radius at high HF exchange contents. The CrPB optimizations provide useful comparisons, though we are mindful of the fact that the lattice constant used is not expected to accurately represent this compound. We find Fe^{3+}—N bonds in PB that are 0.02–0.03 Å longer than the Cr^{3+}—N bonds in CrPB, while an opposite trend prevails in the Fe^{2+}—C distances. Finally, we note that the C≡N bond lengths are relatively well determined by all methods and are similar in both materials.

B. Charges

Table II presents the ionic charges obtained from Mulliken population analyses. The results must be interpreted with caution, and should be regarded only to establish relative variations, for the absolute values are known to bear little formal meaning and to display strong basis set dependence.[31] Bearing these limitations in mind, we observe that the magnitudes of all charges increase steadily as the limit of pure HF exchange is approached, indicating a trend toward a more ionic character of bonding at high F_0 values. This interpretation is supported by the steady reduction in the overlap populations across the same range. The charges borne by the HS Fe and Cr ions are approximately $+1|e|$

TABLE II. The total charges (e) and spin moments (μ_B) borne by the atoms spanning the J_2-exchange pathway in both FM and AF_2 PB and CrPB at $F_0=35\%$ and $F_0=100\%$.

F_0	Material	State	HS metal	N	C	LS Fe	C	N	HS metal
					Charges				
35	PB	FM	+2.33	−0.65	−0.10	+1.20	−0.10	−0.65	+2.33
100			+2.53	−0.76	−0.06	+1.35	−0.06	−0.76	+2.53
35	CrPB		+2.02	−0.60	−0.11	+1.23	−0.11	−0.60	+2.02
100			+2.19	−0.70	−0.06	+1.38	−0.06	−0.70	+2.19
					Spin moments				
35	PB	FM	+4.48	+0.05	+0.03	+0.05	+0.03	+0.05	+4.48
		AF_2	−4.47	−0.06	−0.03	0.00	+0.03	+0.06	+4.48
100		FM	+4.72	+0.03	+0.01	0.00	+0.01	+0.03	+4.72
		AF_2	−4.72	−0.04	−0.01	0.00	+0.01	+0.03	+4.72
35	CrPB	FM	+2.96	−0.06	+0.06	+0.04	+0.06	−0.06	+2.96
		AF_2	+2.96	−0.06	+0.06	0.00	−0.06	+0.06	−2.96
100		FM	+3.00	−0.07	+0.07	0.00	+0.07	−0.07	+3.00
		AF_2	+3.00	−0.07	+0.07	0.00	−0.07	+0.07	−3.00

greater than those on LS Fe sites, in keeping with the differences in their formal oxidation states, but we note that the individual magnitudes all lie well below the respective formal values. The detailed breakdown of TM d-orbital populations presented in Table III offers further insight, revealing t_{2g}-orbital occupations appropriate to the formal charge in each case, while the e_g populations are consistently greater than expected, particularly in the case of the Fe^{2+} ion. The underestimation of the TM charges would therefore seem to be due to the occupation of the latter orbitals, which we attribute to their substantial overlap with the ligand lone pairs. For the sake of consistency, however, we continue to refer to the TM sublattices by their notional oxidation states throughout this study.

C. Spin moments

The atomic spin moments presented in Table II are important quantities bearing directly upon saturation magnetizations and the magnitudes of the magnetic energy differences. While the present approach includes only the contributions due to spin, the values reported remain comparable with experiment, for the orbital component in first row TM compounds is normally quenched by strong ligand field interactions.[32] The high F_0 functionals yield Fe^{3+} and Cr^{3+} moments close to the spin-only free ion values of $5\mu_B$ and $3\mu_B$, respectively, with unpaired e_g and t_{2g} populations as shown in Table III approaching the configurations expected in the isolated limit. The moments borne by the former ion steadily decrease as HF exchange content falls, while the latter remain relatively constant. We attribute the difference in behavior to the general increase in total e_g populations as F_0 is reduced, which leads to more spin pairing in the Fe^{3+} ion. Meanwhile, the alignments and magnitudes of the smaller moments borne by the ligand atoms vary with a number of factors, namely, the HF exchange content of the functional, the magnetic state, and the identity of the coordinating TM species. More specifically, the moments on C and N atoms align in parallel with the spin of the nearest Fe^{3+} site in each state of PB, while in CrPB, the N moments align antiparallel to the nearest-neighbor Cr^{3+} spin, and the C moments antiparallel, in turn, to the neighboring N spin.

The small spin densities manifesting on the LS Fe^{2+} sites are of particular interest for the insight they provide into the exchange coupling mechanism. We find that this ion is com-

TABLE III. The total and spin-polarized populations of the TM e_g and t_{2g} orbitals in FM PB and CrPB at $F_0=35\%$ and $F_0=100\%$.

		Total population		Spin-polarized population	
F_0	Material	M^{3+} e_g, t_{2g}	Fe^{2+} e_g, t_{2g}	M^{3+} e_g, t_{2g}	Fe^{2+} e_g, t_{2g}
35	PB	2.42, 3.11	1.31, 5.36	1.62, 2.84	0.01, 0.04
100		2.31, 3.04	0.76, 5.79	1.77, 2.94	0.00, 0.00
35	CrPB	0.84, 3.03	1.23, 5.41	0.12, 2.83	−0.01, 0.05
100		0.67, 3.03	0.71, 5.81	0.07, 2.92	−0.01, 0.01

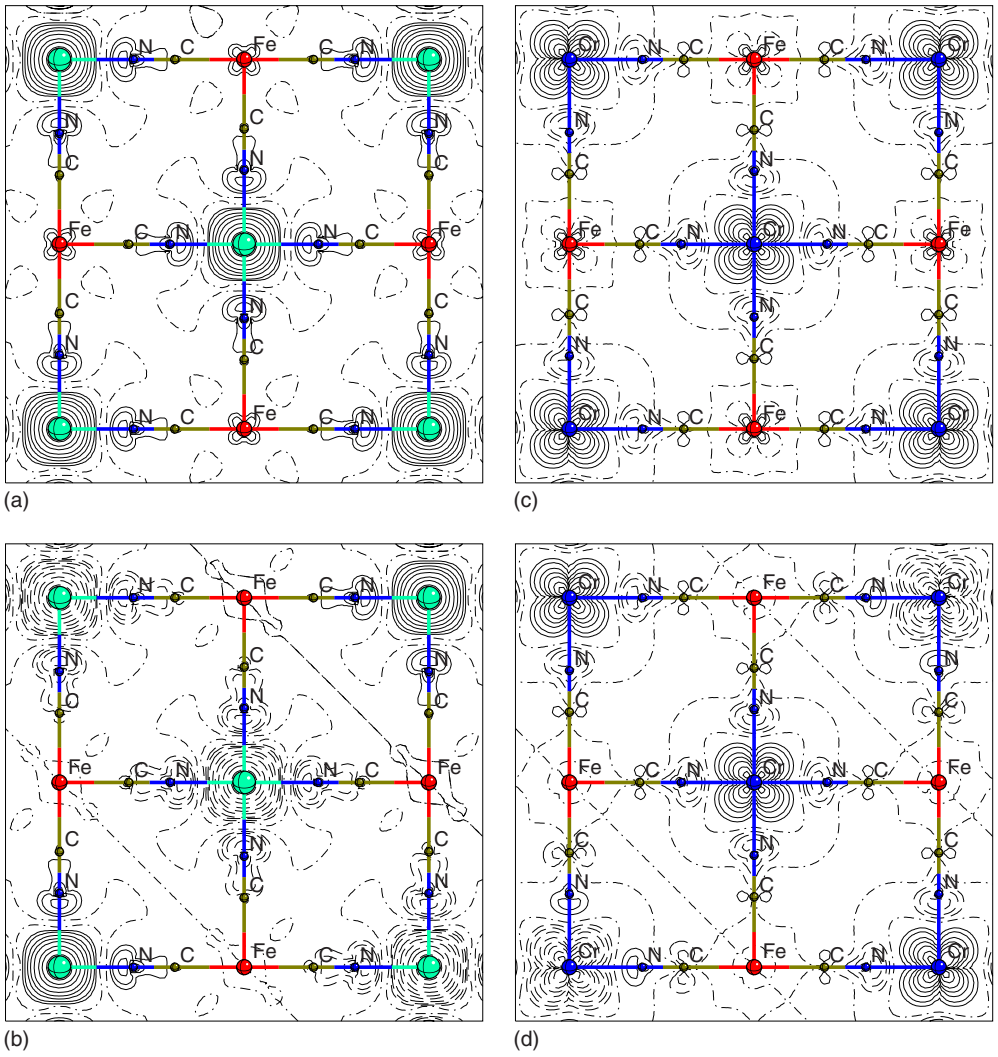

FIG. 3. (Color online) Projections onto the (100) plane of the F_0=35% spin densities in (a) FM PB, (b) AF_2 PB, (c) FM CrPB, and (d) AF_2 CrPB plotted on a logarithmic scale. Solid, dashed, and dot-dashed lines denote positive, negative, and zero valued contours, respectively.

pletely spin paired in AF_2 PB, while small moments ranging from $0.002\mu_B$ to $0.070\mu_B$ at the UHF and F_0=30% limits, respectively, are observed in the FM ground state. The latter value is in good agreement with the limit of 5% of an electron obtained from the spin-polarized neutron diffraction study of Day *et al.*[14] We note also that the HS Fe^{3+} and LS Fe^{2+} moments coalign in the FM state, the spin polarization at the latter sites residing primarily in the t_{2g} orbitals, as shown in Table III. The spin-delocalization model of the J_2 interactions advanced previously suggests that it is only the minority spin density borne by Fe^{2+} ions that may delocalize onto Fe^{3+} sites, producing remnant majority spin moments in the Fe^{2+} t_{2g} states.[15] The calculated electronic structure supports this model, suggesting that long-range spin-delocalization effects are present in PB. Moreover, the observation of a qualitatively similar behavior in CrPB leads us to conclude that a delocalization-mediated coupling of the HS Cr^{3+} moments operates in this material also. However, the FM Fe^{2+} moments are slightly lower in this case, increasing from zero to $0.050\mu_B$ across the range from UHF to F_0 =30%. We note that the present spin-delocalization mechanism shares some similarities with the well-known double exchange (DE) interaction proposed for Fe_3O_4 and other mixed valence TM compounds.[32] However, as a class-II mixed valence system, PB lacks the metallic ground state characteristic of the true DE materials.

Finally, Fig. 3 presents plots of the FM and AF_2 spin densities projected onto the (100) planes of both compounds. The distributions of spin are in agreement with the Mulliken analyses shown earlier and, regardless of sign, are of nearly identical form in both states. The interpretation of the plots is assisted by a further Mulliken partitioning of the ligand spin populations into (s, p_σ, and p_π) orbital contributions. We obtain values at F_0=35% of

$$\mathrm{N} \quad (0.028,\ 0.023,\ 0.002)\mu_B$$

and

$$\mathrm{C} \quad (0.002,\ 0.006,\ 0.016)\mu_B,$$

respectively, in FM PB, and

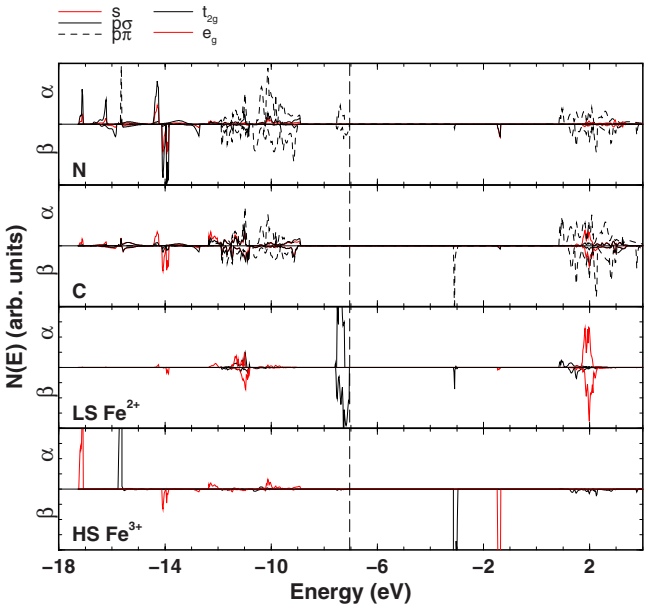

FIG. 4. (Color online) The atom-projected densities-of-states plots in FM PB at $F_0=35\%$. Spin-up (α) and spin-down (β) states are shown separately in each pane. The leftmost legend applies to the C and N panes, and the rightmost to the LS Fe^{2+} and HS Fe^{3+} panes. The dashed vertical line denotes the valence band edge.

$$\mathrm{N} \quad (-0.014,\ -0.010,\ -0.038)\mu_B$$

and

$$\mathrm{C} \quad (0.004,\ -0.001,\ 0.058)\mu_B,$$

respectively, in FM CrPB. The combination of these results with the TM orbital occupations presented earlier, leads to the conclusion that the observed ligand spin polarization in PB arises out of the overlap of HS Fe^{3+} e_g orbitals with ligand σ orbitals, and out of π overlap with Cr^{3+} t_{2g} orbitals in CrPB.

D. Electronic structure and densities of states

The atom- and orbital-projected densities-of-states plots obtained in FM PB at $F_0=35\%$ are presented in Fig. 4. We observe uppermost valence bands dominated by Fe^{2+} $t_{2g}(\beta)$ states with some small admixture of N p_π states, while the lowermost conduction bands comprise a majority of Fe^{3+} $t_{2g}(\beta)$ states in combination with a minority weight of C $p_\pi(\beta)$ states. Consequently, the fundamental excitation of the system in this Hamiltonian corresponds to a spin-allowed $Fe^{2+} \rightarrow Fe^{3+}$ intervalence charge transfer, in agreement with the conclusions drawn from the previous spectroscopic studies.[33] A closer examination of the valence band edge (VBE) reveals that the Fe^{2+} $t_{2g}(\beta)$ band is 0.23 eV wider than the corresponding α-spin band, suggestive of an increased delocalization of the minority spins in keeping with the prevailing model of the J_2 couplings.[15]

Optical absorption experiments in K^+-doped PB obtain a peak at 686 nm, corresponding to an excitation energy of 1.81 eV.[34] The gap of width 3.87 eV obtained from the $F_0=35\%$ calculation represents a clear overestimation of this experimental value, while the previous pure PW91 functional calculations of Wojdeł and Bromley[22] produced a narrower gap of width 1.15 eV. An improved agreement with the experimental spectra might therefore be expected from a hybrid functional containing an intermediate weight of HF exchange. The B3LYP method (equivalent to $F_0=20\%$) is of particular interest in this regard, given previous demonstrations that it provides band gaps in good agreement with experiment in a wide range of materials.[35,36] Unfortunately, as noted earlier in Sec. II, we were unable to obtain a converged ground state for this functional in the present study.

The ligand p_π-derived states fall in a broad range of energies from 2 to 5 eV below the VBE. The states associated with the C lone pair partially overlap the p_π bands in a range from 4 to 5 eV below the VBE, while the N lone pair states lie in a narrow band 2–3 eV lower still. The downward shift of these states from their position above the π orbitals in the isolated CN^- anion can be attributed to their strong interaction with the TM cations. The occupied Fe^{3+} states, meanwhile, appear in the range from 8.5 to 10.5 eV below the VBE. Interestingly, the e_g states lie approximately 1.5 eV below the t_{2g} band; this apparent contradiction of the crystal field model again arises out of the strong metal-ligand interactions. Finally, we note that the model for the ligand spin polarization advanced in Sec. III C is supported by the presence of N $s(\alpha)$ and $p_\sigma(\alpha)$ states at energies coincident with the Fe^{3+} $e_g(\alpha)$ states. However, the close proximity of a smaller N $p_\pi(\alpha)$ peak to the Fe^{3+} $t_{2g}(\alpha)$ states may indicate some contributions due to π overlap.

E. Spin transitions

The findings of the preceding sections pertain to lattices bearing LS Fe^{2+} and HS Fe^{3+} ions, but it remains to be determined whether these configurations are featured in the ground state of each Hamiltonian. The relative stabilities of the various TM spin states are also of interest from the perspective that, as in the photomagnetic materials,[1] metastable excited states at accessible energies may lead to the appearance of novel magnetic properties. We therefore seek the most stable HS Fe^{2+} ($S=2$) and LS Fe^{3+} ($S=\frac{1}{2}$) states, which it is anticipated will involve configurations featuring one doubly and one singly occupied orbital, respectively. These states cannot be represented within the full $F\bar{4}3m$ space group, and so the symmetry of the cells is lowered by the application of an infinitesimal tetragonal distortion along the z direction. We consider the following set of symmetry-consistent configurations for the Fe^{2+} HS ($S=2$) state:

$$\text{HS } Fe^{2+}(xy) \qquad z^2(\uparrow)xz(\uparrow)yz(\uparrow)x^2-y^2(\uparrow)xy(\uparrow\downarrow),$$

$$\text{HS } Fe^{2+}(xz/yz) \quad z^2(\uparrow)xz\left(\uparrow+\tfrac{1}{2}\downarrow\right)yz\left(\uparrow+\tfrac{1}{2}\downarrow\right)x^2-y^2(\uparrow)xy(\uparrow),$$

$$\text{HS } Fe^{2+}(x^2-y^2) \quad z^2(\uparrow)xz(\uparrow)yz(\uparrow)x^2-y^2(\uparrow\downarrow)xy(\uparrow),$$

$$\text{HS } Fe^{2+}(z^2) \qquad z^2(\uparrow\downarrow)xz(\uparrow)yz(\uparrow)x^2-y^2(\uparrow)xy(\uparrow).$$

As in recent work on the $d \rightarrow d$ excitations in the TM oxides,[35,37,38] we apply the Kanamori Hamiltonian[39] to de-

TABLE IV. The variation with F_0 in the energies (eV f.u.$^{-1}$) of the Fe^{2+} LS→HS(xy) and Fe^{3+} HS →LS(xy) transitions in the fixed ground state (Fix) and optimized excited state (Opt) structures, along with the associated relaxation energies, E_{Relax}.

	$KFe^{3+}[Fe^{2+}(CN)_6]$						$KCr^{3+}[Fe^{2+}(CN)_6]$		
	$\Delta E Fe^{2+}$ LS→HS(xy)			$\Delta E Fe^{3+}$ HS→LS(xy)			$\Delta E Fe^{2+}$ LS→HS(xy)		
F_0	Fix	Opt	E_{Relax}	Fix	Opt	E_{Relax}	Fix	Opt	E_{Relax}
35	4.28	2.98	1.30	1.54	1.05	0.48	3.57	2.41	1.17
40	3.95	2.69	1.26	1.72	1.28	0.43	3.25	2.14	1.11
50	3.25	2.14	1.11	1.99	1.50	0.49	2.63	1.65	0.98
60	2.60	1.67	0.93	2.25	1.81	0.43	2.07	1.20	0.87
70	2.09	1.26	0.83	2.54	2.08	0.46	1.59	0.83	0.77
80	1.63	0.90	0.73	2.83	2.39	0.45	1.18	0.49	0.69
90	1.23	0.58	0.66	3.12	2.69	0.43	0.80	0.19	0.62
100	0.88	0.29	0.60	3.40	2.98	0.42	0.49	−0.07	0.56
UHF	0.34	−0.24	0.58	4.12	3.72	0.40	−0.03	−0.58	0.55

rive expressions for the energies of these configurations in terms of crystal field (E_{CF}) splittings, intra- and interband Coulomb (E_C) interactions, and interband exchange (E_X) interactions. Like terms grouped together, we obtain total contributions as follows:

$E[Fe^{2+}LS]$:

$$E_C = 15A - 12B + 21C, \quad E_X = -18B - 6C, \quad E_{CF} = 0,$$

$E[Fe^{2+}HS(xy)] = E[Fe^{2+}HS(xz/yz)]$:

$$E_C = 15A - 10B + 17C, \; E_X = -24B - 9C, \; E_{CF} = 2\Delta_{CF},$$

$E[Fe^{2+}HS(x^2-y^2)] = E[Fe^{2+}HS(z^2)]$:

$$E_C = 15A - 10B + 17C, \; E_X = -24B - 9C, \; E_{CF} = 3\Delta_{CF},$$

where A, B, and C denote the well-known Racah parameters,[40] and Δ_{CF} the crystal field splitting energy. It is clear that the HS(e_g) states are of sufficiently high energy that they need not be considered further. Moreover, the degeneracy of the HS(t_{2g}) states means that the properties of only one representative configuration need be determined; we select the HS(xy) state for this purpose. The purely electronic part of the Fe^{2+} LS→HS(xy) transition energy within the fixed ground state geometry is directly obtained from the difference in the appropriate configuration energies as

$$\Delta E Fe^{2+}LS \rightarrow HS(xy) = 2\Delta_{CF} - 4B - 7C,$$

with

$$\Delta E_C = 2B - 4C, \quad \Delta E_X = -6B - 3C, \quad \Delta E_{CF} = 2\Delta_{CF},$$

corresponding to the vertical excitation within the Franck–Condon model. Thus, the excited state will be further stabilized by relaxation of the local lattice, lowering the energy by an amount E_{Relax}.

It is useful to derive some estimates for the individual components of the excitation energy. Sugano *et al.*[41] reported values of 0.114 eV and 4.41 for B and ratio C/B, respectively, in the free ion, the substitution of which led to negative values for ΔE_C and ΔE_X, favoring the HS Fe^{2+} state. This is a reasonable finding given that an essentially identical set of interactions underlie Hund's first rule, which establishes that the ground state term of the free atom possesses maximum multiplicity. However, we must also consider that the Fe^{2+} ions in PB experience a strong crystal field, which will tend to favor the formation of a LS state. By taking the values quoted for B and C/B (Ref. 41) in combination with a nephelauxetic factor of approximately 0.5 for ferricyanide compounds,[42] we predict a LS Fe^{2+} ground state for Δ_{CF} values greater than approximately 1 eV. We note that a much higher Δ_{CF} value of 4.07 eV has been obtained previously in the LS $Fe^{2+}(CN)_6$ complex.[43]

Turning to examine the Fe^{3+} HS→LS transition, a similar analysis indicates that the three degenerate LS(t_{2g}^5) states will be the most stable $S=\frac{1}{2}$ configurations. The configuration with a singly occupied xy orbital taken as representative, we obtain a vertical excitation energy

$$\Delta E Fe^{3+}HS \rightarrow LS(xy) = 15B' + 10C' - 2\Delta'_{CF},$$

with

$$\Delta E_C = 2B' + 4C', \quad \Delta E_X = 13B' + 6C', \quad \Delta E_{CF} = -2\Delta'_{CF},$$

where the parameters are primed to distinguish them from those used for the Fe^{2+} site above. Again, we see that ΔE_C and ΔE_X both favor the HS state. Griffith provides a value of 0.135 eV for the B' parameter in the free ion,[40] which, taken together with an estimate of 4.4 for the ratio C'/B' and a nephelauxetic factor of 0.5,[42] leads us to predict a HS Fe^{3+} ground state for Δ'_{CF} values of approximately 2 eV and less. A stabilization due to structural relaxation is expected in this case also.

The relative stabilities of the spin states have been shown to depend on the complex interplay of the Racah parameters, crystal field splittings, and relaxation energies. More quantitative treatments require the intervention of direct calculations, the results of which are presented in Table IV and Fig. 5. We first examine the Fe^{2+} LS→HS(xy) data, finding that

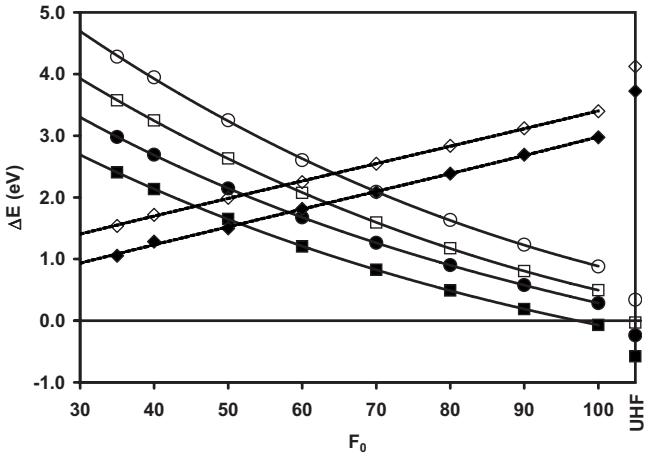

FIG. 5. Energy as a function of F_0 of the Fe^{2+} LS→HS(xy) transition in PB (○) and CrPB (□), and the Fe^{3+} HS→LS(xy) transition in PB (◇), both with (filled) and without (unfilled) relaxation of the excited state structure.

the LS states become progressively more stable as F_0 is reduced and that, save in CrPB at the UHF level, the vertical excitation energies are all positive, favoring the experimentally observed LS Fe^{2+} state.[14] The relaxation of the excited state structures yields only marginal changes, stabilizing HS Fe^{2+} ground states at the UHF level in both compounds and at F_0=100% in CrPB. We note also that comparable Fe^{2+} LS→HS(xy) excitation energies differ substantially in PB and CrPB, indicating a significant coupling of the transitions to the crystal environment. The lower transition energies in CrPB are likely due to the reduced crystal field splittings accompanying the longer Fe^{2+}—C bonds in this case.

The Fe^{3+} HS→LS(xy) results differ significantly, most notably in that the excitation energies decrease as F_0 is reduced. The energies are positive in all Hamiltonians, favoring the experimentally observed Fe^{3+} HS ground state. Interestingly, we note that the trend lines for the Fe^{3+} HS→LS and Fe^{2+} LS→HS transitions cross for F_0 values of approximately 50%–70%, so that the former is lower in energy below this range, and the latter above. We cannot at this point decide which of these alternatives is the more realistic. However, it is anticipated that comparisons with experimental and theoretical data for the spin transitions in other Fe compounds may reveal which of our Hamiltonians is the more reliable in this regard. We pursue this matter further in Sec. IV and limit our present conclusions to the fact that the experimentally observed HS Fe^{3+} and LS Fe^{2+} configurations are stable across a wide range of HF exchange contents.

Finally, we discuss the changes in energy and structure accompanying the relaxation of the excited states. The stabilizations of the Fe^{2+} HS(xy) states are similar in both PB and CrPB, and increase progressively as F_0 falls. We find that the Fe^{2+}—C bonds elongate by amounts ranging from 0.08 to 0.11 Å due to the occupation of the antibonding e_g orbitals, while the Fe^{3+}—N and Cr^{3+}—N bonds shorten correspondingly. In contrast, the relaxation-induced stabilizations of the Fe^{3+} LS(xy) states are much smaller and appear relatively insensitive to variations in the Hamiltonian. The Fe^{3+}—N bonds in this case shorten by 0.07 to 0.08 Å due to the vacation of the e_g orbitals, while the Fe^{2+}—C bonds elongate correspondingly. A close examination of the optimized structures of both excited states reveals bond lengths in the xy plane slightly differing from those oriented along the z axis, in keeping with the fact that the HS d^6 and LS d^5 configurations are both weakly Jahn–Teller active. We end with the important caveat that our treatment of the spin transitions uses fixed cells, and that the effects on the excitation energies of changes in the lattice constant consequently remain undetermined. It is possible that these stabilizations may be substantial, given that the metal-ligand bond lengths d vary close to linearly with cell length, and that Δ_{CF} varies as d^{-5} in the simple crystal field model.

TABLE V. The number of nn and nnn HS moments aligned parallel (↑↑) and antiparallel (↑↓) to any given HS moment in the FM, AF_1, and AF_2 orders.

Spins	FM	AF_1	AF_2
nn ↑↑	12	4	6
nn ↑↓	0	8	6
nnn ↑↑	6	6	0
nnn ↑↓	0	0	6

F. Magnetic coupling constants

We now provide a fuller description of the magnetic states used in the calculation of the coupling constants. The AF_1 order incorporates {100} planes of parallel spin antiferromagnetically aligned along the corresponding ⟨100⟩ normal direction, where the Miller indices refer to the cubic conventional cell. We represent this state within a bimolecular supercell defined by the vectors $\mathbf{a}'=\mathbf{a}+\mathbf{b}-\mathbf{c}$, $\mathbf{b}'=\mathbf{c}$, and $\mathbf{c}'=\mathbf{a}-\mathbf{b}$, where $\mathbf{a}$, $\mathbf{b}$, and $\mathbf{c}$ are the lattice vectors of the rhombohedral primitive cell. Similarly, the AF_2 lattice antiferromagnetically aligns {111} planes of parallel spin along the appropriate ⟨111⟩ normal, within a supercell delimited by vectors $\mathbf{a}'=\mathbf{b}+\mathbf{c}$, $\mathbf{b}'=\mathbf{a}+\mathbf{c}$, and $\mathbf{c}'=\mathbf{a}+\mathbf{b}$. The FM order can, in principle, be established within a cell of arbitrary size. However, in the present work, it is always represented within the AF_2 supercell, so as to avoid the introduction into the coupling constants of any numerical errors arising from the use of varying cell sizes. The magnetic environments of the three states are listed in Table V. The coupling constants, J_1 and J_2, are obtained from the mapping of the energies of the FM, AF_1, and AF_2 states onto an Ising Hamiltonian of the form

$$H_{\mathrm{Spin}} = -\frac{1}{2}J_1\sum_{ij}^{nn}\sigma_i\sigma_j - \frac{1}{2}J_2\sum_{ij}^{nnn}\sigma_i\sigma_j,$$

where σ_i and σ_j are both either HS Fe^{3+} ($S=\frac{5}{2}$) or Cr^{3+} ($S=\frac{3}{2}$) spin moments, and in which the first sum runs over the 12 sites nn to each HS TM ion, and the second over the 6 next-nearest-neighbor (nnn) sites. Positive J values favor the FM state within this sign convention. Expressions for the energies per HS ion of the FM, AF_1, and AF_2 states can be

TABLE VI. The variation with F_0 in the character of the ground magnetic state, magnetic energy differences (10^{-6} hartree per HS TM ion), exchange interaction strengths, J_1 and J_2 (K), ratio $x=J_1/J_2$, and critical temperature corrected for fluctuations and stoichiometry, T_C (K), in PB and CrPB. Experimental value from Ref. 13.

	$KFe^{3+}[Fe^{2+}(CN)_6]$							$KCr^{3+}[Fe^{2+}(CN)_6]$						
F_0	State	$E_{AF_2}-E_{FM}$	$E_{AF_1}-E_{FM}$	J_1	J_2	x	T_C	State	$E_{AF_2}-E_{FM}$	$E_{AF_1}-E_{FM}$	J_1	J_2	x	T_C
30	FM	65.47	55.90	0.3530	0.1983	1.78	9.54	FM	79.39	80.72	1.4162	0.4409	3.21	12.43
35	FM	40.75	35.49	0.2241	0.1190	1.88	5.98	FM	66.00	65.99	1.1578	0.3861	3.00	10.26
40	FM	25.73	22.83	0.1442	0.0725	1.99	3.81	FM	54.68	53.88	0.9452	0.3337	2.83	8.44
50	FM	10.56	9.64	0.0609	0.0280	2.17	1.58	FM	37.38	35.87	0.6293	0.2452	2.57	5.71
60	FM	4.46	4.02	0.0254	0.0122	2.08	0.66	FM	25.86	24.01	0.4212	0.1836	2.29	3.90
70	FM	1.84	1.61	0.0102	0.0053	1.92	0.27	FM	18.06	16.01	0.2809	0.1415	1.99	2.67
80	FM	0.63	0.47	0.0030	0.0023	1.29	0.09	FM	12.58	10.49	0.1840	0.1103	1.67	1.82
90	AF_1	0.07	−0.06	−0.0004	0.0010	−0.39	0.01	FM	9.08	6.94	0.1218	0.0907	1.34	1.27
100	AF_1	−0.20	−0.28	−0.0018	0.0000	−53.75	0.01	FM	6.41	4.15	0.0728	0.0770	0.95	0.85
UHF	FM	0.29	0.33	0.0021	0.0004	5.01	0.05	FM	18.78	16.52	0.2898	0.1496	1.94	2.77
Expt.	FM						5.6							

derived from the spin alignments of HS ions in the nn and nnn shells shown in Table V, yielding values of $E_0-6J_1\sigma^2-3J_2\sigma^2$, $E_0+2J_1\sigma^2-3J_2\sigma^2$, and $E_0+3J_2\sigma^2$, respectively, where E_0 is the energy of the paramagnetic (PM) state. The coupling constants are then obtained from these energies as

$$J_1=\frac{1}{8\sigma^2}(E_{AF_1}-E_{FM}),$$

$$J_2=\frac{1}{6\sigma^2}(E_{AF_2}-E_{FM})-J_1.$$

Finally, the critical temperature for the transition from spin order to paramagnetism can be estimated as $T_C\approx(E_0-E_{Ord})/k_B$, where E_{Ord} is the energy of the appropriate ordered state presented above. An approximate correction for the effect of fluctuations can be made by multiplying T_C by the factor $\frac{3}{4}$ obtained from Monte Carlo simulations of cubic spin lattices.[44] We may also account for the presence of the water molecules and $Fe^{2+}(CN)_6$ vacancies in the experimental structure by multiplying our theoretical T_C value by a further factor of $\frac{3}{4}$ derived from the average stoichiometry. The validity of adjusting the critical temperature in this way was established by our previous combined experimental and theoretical study of the $Mn_3[Cr(CN)_6]_2\cdot 16H_2O$ PBA.[25]

Table VI and Fig. 6 present the magnetic energy differences, coupling constants, and estimated critical temperatures obtained in PB and CrPB. It is immediately clear that the FM ground state is favored for each value of F_0 in both compounds, save in PB at F_0 values of 90% and 100%, where antiferromagnetic nn interactions stabilize AF_1 ground states. In general, though, the parallel spin alignment observed in PB by neutron diffraction[14] is favored across a wide range of Hamiltonians. While the $F_0=35\%$ J_1 and J_2 values of 0.019 and 0.010 meV, respectively, in PB, and 0.100 and 0.033 meV, respectively, in CrPB, are certainly small, they are comparable to the weak interactions in NiF_2 and MnF_2, which were well treated by previous $F_0=35\%$ calculations.[30] The coupling constants obtained from the other Hamiltonians are similarly precise, but are not expected to be as accurate as the $F_0=35\%$ values and should be regarded solely to establish trends across the range of HF exchange contents. The uncertainties due to incomplete convergence presented in Sec. II must also be borne in mind when considering these results.

An examination of the ratio $x=J_1/J_2$ over the range $30\%\leqslant F_0\leqslant 80\%$ in which FM PB is stable reveals that the J_1-type coupling is approximately 1.3–2.2 times stronger than the long-range J_2 interaction. Given an energy difference per HS site of $(6J_1+3J_2)\sigma^2$ separating the FM and PM state, we see that the contribution of the nn (J_1) coupling to the stability of the FM state with respect to disorder is 2.6–4.4 times greater than that due to nnn (J_2) interactions. Thus, it would seem that the previous model of the magnetic coupling in PB including only J_2-type interactions[15] is incomplete. The current results point to a more complex picture, in

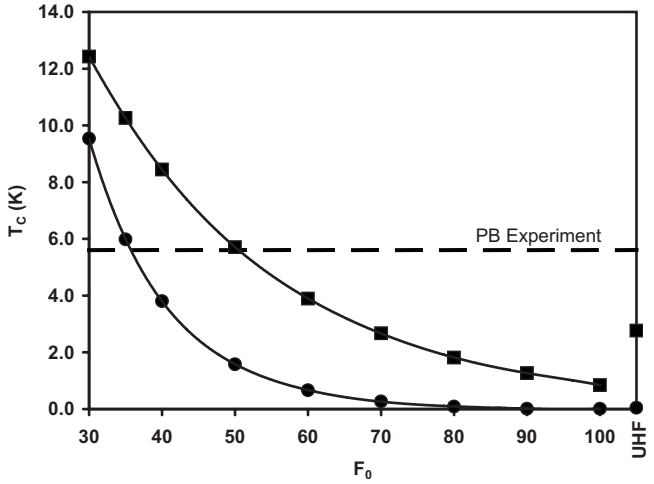

FIG. 6. Fluctuation- and stoichiometry-corrected critical temperatures (K) of PB (●) and CrPB (■) for varying values of F_0. Experimental value from Ref. 13.

TABLE VII. The variation with lattice constant, a_0 (Å), in the FM band gap, ΔE_g (eV), exchange interaction strengths, J_1 and J_2 (K), ratio $x=J_1/J_2$, and estimated critical temperature, T_C (K), in PB at $F_0=35\%$.

a_0	State	ΔE_g	J_1	J_2	x	T_C
10.35	FM	3.823	0.1980	0.1045	1.89	5.28
10.28	FM	3.870	0.2241	0.1190	1.88	5.98
10.20	FM	3.951	0.2566	0.1342	1.91	6.83
10.13	FM	4.037	0.2853	0.1509	1.89	7.61
10.06	FM	4.158	0.3169	0.1671	1.90	8.45

which both types of interactions significantly contribute to the ground state. We observe that the coupling constants increase as F_0 falls, so that the estimated critical temperatures, which are too low at high contents of HF exchange, come into good agreement with the experimental value of 5.6 K (Ref. 13) for F_0 values in the range from 35%–40%. The results obtained for CrPB are similar, save that the coupling constants and their ratios are generally larger in this case. The enhancement in magnetism is due to the increased orbital overlap and weakening of the on-site interactions accompanying the more extended $3d$ orbitals in the early TM cations.[45]

Finally, given that the previous experimental studies report a wide range of structural parameters for PB,[3,9–11] we investigate the variations in the magnetic interaction strengths and FM band gap width with lattice constant. The $F_0=35\%$ results presented in Table VII reveal trends in J_1 and J_2 that are very close to linear across the range from 10.06 to 10.35 Å, with corresponding gradients of −0.410 and −0.215 K Å^{-1}, respectively. A decrease in the lattice constant from 10.28 to 10.13 Å raises the critical temperature by approximately 1.6 K, or 29% of the experimental value, leading us to conclude that the choice of structural parameters is important if quantitative results are sought. However, we note that the ratio of the interaction strengths is nearly constant across the range, indicating that our earlier findings with regard to the relative contribution of the two types of coupling remain unchanged by a variation in structure. The band gap widths are also found to significantly increase as the lattice contracts.

IV. DISCUSSION

The variations with weight of HF exchange in ionic charges and spin moments within the current work are similar to those obtained in previous studies of the TM oxides.[35,37,38] The more significant results of our investigation are related to the demonstration that hybrid functionals can provide an accurate representation of mixed valence compounds bearing LS ions. The agreement between the PB experimental data and the results obtained at F_0 values of approximately 35% merits particular mention. Calculations within this regime obtain a FM ground state in which the Fe^{2+} and Fe^{3+} ions adopt LS and HS configurations, respectively, with a delocalization of spin density onto the Fe^{2+} sites in good agreement with the experimental data in terms of both magnitude and sign. Furthermore, the experimental and estimated theoretical FM→PM critical temperatures coincide for a F_0 value in the range from 35% to 40%. The latter result is particularly encouraging, for it extends the range of successful applications of the $F_0=35\%$ functional from the more conventional TM compounds with short exchange pathways[30] to the present systems, in which weak couplings are conveyed over much longer distances. Of greater significance is the finding that the FM PB ground state is stabilized more by the interactions between nn HS Fe^{3+} sites than by the delocalization of spin along the $\cdots$NC—Fe^{2+}—CN$\cdots$ pathways. We suggest on this basis that the magnetism of PB at pressure may be of interest, for, assuming normal Bethe–Slater behavior, the nearest-neighbor couplings would be expected to eventually become antiferromagnetic as the lattice contracts.[46] However, it must be borne in mind that the present calculations offer no direct insight into the mechanism underlying the J_1 couplings. We therefore remain open to the possibility that these interactions may not proceed by a direct overlap of HS metal orbitals but, rather, by exchange through right-angled $\cdots$NC—Fe^{2+}—CN$\cdots$ pathways.

Also of interest is the finding that the couplings in CrPB are more strongly ferromagnetic than those in PB, despite the fact that the interactions between d^3 centers through single ligand bridges in the PBAs are very strongly antiferromagnetic.[3] While we should be wary of inferences drawn from a study of just two materials, it is possible that the nature of the ground magnetic state in these systems does not strongly depend on the HS TM species present. The model for the spin delocalization in CrPB is necessarily more complex than that in PB, for the presence of the unoccupied Cr^{3+} e_g orbitals offers the possibility of both majority and minority spin transfer from Fe^{2+} to Cr^{3+} sites. An analysis within the Kanamori Hamiltonian,[39] as in Sec. III E, yields changes in configuration energies of $3A-6B+\Delta_{CF}$ for the $Cr^{3+}(t_{2g}^3)\rightarrow Cr^{2+}(t_{2g}^3 e_g^1)$ electron addition, and $3A+5C$ for the $Cr^{3+}(t_{2g}^3)\rightarrow Cr^{2+}(t_{2g}^4)$ addition. Reasonable estimates of the B, C, and Δ_{CF} parameters favor a majority spin transfer into the $Cr^{2+}(t_{2g}^3 e_g^1)$ state, but the results obtained from direct calculations disagree with this simple analysis, revealing small moments on the Fe^{2+} sites aligned parallel to those on the HS Cr^{3+} ions. A more general insight into the J_2-type coupling must therefore await further studies of similar materials bearing a wide range of HS TM cations.

Turning to discuss the spin transitions, we start by noting that the relative energies of the TM spin states can be use-

fully reinterpreted on the basis of the ability of the various Hamiltonians to account for pair correlation effects. Wilson *et al.*[47] provided a discussion along these lines in their recent hybrid functional study of ilmenite ($FeTiO_3$). A similar analysis of the present materials proceeds on the basis that the Fe^{2+} ion manifests one and three t_{2g} spin pairs in the HS and LS states, respectively, while the same states of the Fe^{3+} ion give rise to zero and two spin pairs, respectively. The stabilizations associated with these interactions can be substantial, with estimates placing the pair correlation energy E_P in the range from 0.2 to 1.3 eV.[48] The relevance of the foregoing emerges from the realization that these correlations are absent within the UHF theory and might be reproduced only in part, if at all, by the various hybrid functionals. Thus, we expect that the LS states will be significantly destabilized in the UHF method, leading to Fe^{2+} LS→HS excitation energies that are underestimated by an amount of the order of $2E_P$ and Fe^{3+} HS→LS energies that are overestimated by a similar margin. More specifically, in the terms used in Sec. III E above, the neglect of the pair correlations leads to gross overestimation of the C and C' Racah parameters. The effect clearly manifests in the large separation of the UHF Fe^{2+} LS→HS and Fe^{3+} HS→LS excitation energies shown in Table IV and Fig. 5. Indeed, for the former transition in CrPB, we find that that the energy of the LS configuration is raised to the extent that it is no longer a part of the ground state. The introduction of the LYP correlation functional at $F_0=100\%$ stabilizes the LS states through the inclusion of some fraction of the pair correlations, and it is clear that this fraction increases progressively as F_0 is reduced. Interestingly, the changes in the excitation energies arising from the variation in F_0 exceed those due to the introduction of the correlation functional. This supports the suggestion made by Wilson *et al.*[47] that the HF exchange content of the functional can be adjusted so as to reproduce the effects of a partially screened self-interaction, with the value $F_0=20\%$ being found to yield properties in good agreement with experiment in ilmenite.[47]

The manifestation of this spin-pairing problem within a range of Fe^{2+} coordination compounds has also been discussed by Daku *et al.*[49] and by Fouqueau *et al.*[50,51] Their studies examined the performance of a variety of functionals for the energy differences and structural changes accompanying spin transitions in the $[Fe(NH_3)_6]^{2+}$ and $[Fe(H_2O)_6]^{2+}$,[50,51] and $[Fe(bpy)_3]^{2+}$ (Ref. 49) complexes. In the first two cases, the best agreement with the CASPT2 and SORCI reference values for the adiabatic HS→LS excitation energy was obtained from calculations employing the VSXC meta-GGA and PBE0 (25% HF exchange) methods.[50,51] The B3LYP (20% exact exchange), B3LYP* (15% exact exchange), and RPBE and HCTH407 pure generalized gradient approximation (GGA) functionals were also found to perform satisfactorily. However, markedly different results were obtained for the LS→HS transition in the $[Fe(bpy)_3]^{2+}$ complex.[49] The B3LYP method in this case produced an excitation energy lying well below the experimental range, while the B3LYP* and RPBE functionals offered values lying just beyond the low and high ends, respectively, of that range. Interpolation suggested that a HF exchange content of approximately 10% was close to optimal in this compound.

The findings of these earlier studies aide in the interpretation of our results, suggesting particularly that the appropriate weight of Fock exchange lies below the stable limit of 35% attained here. Thus, the $F_0=35\%$ energies of 4.28 and 3.57 eV obtained for the vertical Fe^{2+} LS→HS transitions in PB and CrPB, respectively, should be regarded as practical minima, while the value of 1.54 eV for the Fe^{3+} HS→LS transition in the same Hamiltonian can be considered a maximum. The establishment of these limits leads to a number of interesting points. First, given that estimates of the difference in the entropies of the HS and LS Fe^{2+} states are in the range from 0.5 to 0.9 meV K^{-1},[52] we conclude that there is no prospect of a thermally driven spin-crossover effect in PB or CrPB at any reasonable temperature. Second, we note that the estimated energy for the Fe^{3+} HS→LS transition in PB lies below the experimental peak absorption at 1.81 eV and may conceivably be beyond the low energy tail of the band.[34] Although forbidden by the Laporte- and spin-selection rules, this transition may be observable with a weak intensity in spectroscopies sensitive to this region. Third, we observe that the intervalence charge-transfer excitation also generates unpaired spin density on the Fe^{2+} sublattice. The lower energy of this state relative to the Fe^{2+} LS→HS transition renders it a more accessible route toward robust magnetism in PB, but raises questions as to the stability and lifetime of the excitations that, to the best of our knowledge, have not been addressed experimentally.

V. CONCLUSIONS

The current study has shown that hybrid functionals can provide an accurate representation of the key magnetic and electronic properties of mixed valence compounds incorporating LS ions. Our main finding is that the experimentally observed FM ground state in PB is dominated by exchange between nearest-neighbor HS Fe^{3+} ion pairs rather than by the ligand-mediated interactions between next-nearest-neighbor sites as suggested in previous models.[15] Functionals containing weights of HF exchange in the range from 35% to 40% reproduce the experimentally observed LS Fe^{2+} and HS Fe^{3+} configurations, the FM ground state, the weak delocalization of spin onto the Fe^{2+} sites, and the FM→PM transition temperature. The combination of the current results with previous pure GGA calculations[22] leads us to predict that an accurate representation of the intervalence charge transfer excitation may be obtained from functionals incorporating weights of HF exchange close to the well-established B3LYP method.[36]

The variations across the range of functionals in the Fe^{2+} LS→HS and Fe^{3+} HS→LS excitation energies may be understood within a perspective that combines the crystal field model with pair correlation interactions. Comparisons with previous studies of the spin transitions in a range of Fe^{2+} coordination complexes suggest that the appropriate weight of HF exchange for this task lies below the stable minimum of 35% attained here. Nevertheless, this upper limit allows us to conclude that the latter transition occurs with lower energy

than the former, and that there is no reasonable prospect of a temperature-induced spin crossover in either compound.

We recommend that future hybrid functional studies of TM cyanides should include Hamiltonians incorporating weights of HF exchange of 35% and lower. Our future work will consider the magnetism and spin excitations in PB, CrPB, and CuPB at pressure, and will search for stable ground states in hybrid functionals below the present limit of $F_0=30\%$. Direct calculations of the charge-transfer excitation energies will be pursued, and we shall seek an understanding of the variations in properties arising out of the incorporation of $Fe^{2+}(CN)_6$ vacancies and water molecules into the lattices.

ACKNOWLEDGMENTS

The authors thank A. Harrison (Institut Laue-Langevin, France), W. C. Mackrodt (University of St. Andrews, UK), and D. H. Gregory and D. J. Price (University of Glasgow, UK) for useful discussions. The support of the UK EPSRC under Grant No. GR/T21615 is acknowledged.

*c.c.wilson@chem.gla.ac.uk

[1] O. Sato, T. Iyoda, A. Fujishima, and K. Hashimoto, Science **272**, 704 (1996).
[2] E. Coronado, M. C. Gimenez-Lopez, G. Levchenko, F. M. Romero, V. Garcia-Baonza, A. Milner, and M. Paz-Pasternak, J. Am. Chem. Soc. **127**, 4580 (2005).
[3] M. Verdaguer and G. Girolami, in *Magnetism: Molecules to Materials V*, edited by J. S. Miller and M. Drillon (Wiley-VCH, Weinheim, 2004).
[4] L. Egan, K. Kamenev, D. Papanikolaou, Y. Takabayashi, and S. Margadonna, J. Am. Chem. Soc. **128**, 6034 (2006).
[5] A. Kumar and S. M. Yusuf, Physica B **362**, 278 (2005).
[6] S. I. Ohkoshi, Y. Abe, A. Fujishima, and K. Hashimoto, Phys. Rev. Lett. **82**, 1285 (1999).
[7] S. M. Holmes and G. S. Girolami, J. Am. Chem. Soc. **121**, 5593 (1999).
[8] T. Mallah, S. Thiébaut, M. Verdaguer, and P. Veillet, Science **262**, 1554 (1993).
[9] H. J. Buser, A. Ludi, W. Petter, and D. Schwarzenbach, J. Chem. Soc., Chem. Commun. **1972**, 1299.
[10] H. J. Buser, D. Schwarzenbach, W. Petter, and A. Ludi, Inorg. Chem. **16**, 2704 (1977).
[11] F. Herren, P. Fischer, A. Ludi, and W. Halg, Inorg. Chem. **19**, 956 (1980).
[12] K. R. Dunbar and R. A. Heintz, Prog. Inorg. Chem. **45**, 283 (1997).
[13] A. Ito, M. Suenaga, and K. Ono, J. Chem. Phys. **48**, 3597 (1968).
[14] P. Day, F. Herren, A. Ludi, H. U. Gudel, F. Hulliger, and D. Givord, Helv. Chim. Acta **63**, 148 (1980).
[15] B. Mayoh and P. Day, J. Chem. Soc. Dalton Trans. **1976**, 1483.
[16] A. Kumar, S. M. Yusuf, and L. Keller, Phys. Rev. B **71**, 054414 (2005).
[17] N. M. Harrison, B. G. Searle, and E. A. Seddon, Chem. Phys. Lett. **266**, 507 (1997).
[18] J. A. Chan, B. Montanari, W. L. Chan, and N. M. Harrison, Mol. Phys. **103**, 2573 (2005).
[19] E. Ruiz, A. Rodríguez-Fortea, S. Alvarez, and M. Verdaguer, Chem.-Eur. J. **11**, 2135 (2005).
[20] J. C. Wojdeł and S. T. Bromley, Chem. Phys. Lett. **397**, 154 (2004).
[21] J. C. Wojdeł and S. T. Bromley, J. Mol. Model. **11**, 288 (2005).
[22] J. C. Wojdeł and S. T. Bromley, J. Phys. Chem. B **110**, 24294 (2006).
[23] P. A. Christensen, A. Hamnett, and S. J. Higgins, J. Chem. Soc. Dalton Trans. **1990**, 2233.
[24] V. R. Saunders, R. Dovesi, C. Roetti, R. Orlando, C. M. Zicovich-Wilson, N. M. Harrison, K. Doll, B. Civalleri, I. Bush, Ph. D'Arco, and M. Llunell, *CRYSTAL03 User's Manual* (University of Torino, Torino, 2003).
[25] G. Giriat, A. Harrison, D. R. Allan, K. V. Kamenev, and D. S. Middlemiss (Phys. Rev. B to be published).
[26] Crystal basis set library, www.crystal.unito.it
[27] A. D. Becke, Phys. Rev. A **38**, 3098 (1988).
[28] S. H. Vosko, L. Wilk, and M. Nusair, Can. J. Phys. **58**, 1200 (1980).
[29] C. T. Lee, W. T. Yang, and R. G. Parr, Phys. Rev. B **37**, 785 (1988).
[30] X. Feng and N. M. Harrison, Phys. Rev. B **70**, 092402 (2004).
[31] K. B. Wiberg and P. R. Rablen, J. Comput. Chem. **14**, 1504 (1993).
[32] S. Blundell, *Magnetism in Condensed Matter* (Oxford University Press, New York, 2001).
[33] R. J. Mortimer and D. R. Rosseinsky, J. Chem. Soc. Dalton Trans. **1984**, 2059.
[34] D. R. Rosseinsky, H. Lim, X. Zhang, H. Jiang, and J. W. Chai, Eur. Fed. Corros. Publ. **2002**, 2988.
[35] F. Corà, M. Alfredsson, G. Mallia, D. S. Middlemiss, W. C. Mackrodt, R. Dovesi, and R. Orlando, Struct. Bonding (Berlin) **113**, 171 (2004).
[36] J. Muscat, A. Wander, and N. M. Harrison, Chem. Phys. Lett. **342**, 397 (2001).
[37] D. S. Middlemiss and W. C. Mackrodt, Mol. Phys. **103**, 2513 (2005).
[38] W. C. Mackrodt, D. S. Middlemiss, and T. G. Owens, Phys. Rev. B **69**, 115119 (2004).
[39] J. Kanamori, J. Phys. Chem. Solids **10**, 87 (1959).
[40] J. S. Griffith, *The Theory of Transition Metal Ions* (Cambridge University Press, Cambridge, 1964).
[41] S. Sugano, Y. Tanabe, and H. Kamimura, *Multiplets of Transition-Metal Ions in Crystals* (Academic, New York, 1970).
[42] C. K. Jørgensen, *Oxidation Number and Oxidation States* (Springer, New York, 1969).
[43] H. B. Gray, *Electrons and Chemical Bonding* (Benjamin, Menlo Park, 1965).
[44] N. W. Ashcroft and N. D. Mermin, *Solid State Physics* (Harcourt Brace College, Fort Worth, 1976).
[45] P. A. Cox, *Transition Metal Oxides, An Introduction to Their*

Electronic Structure and Properties (Oxford University Press, New York, 1992).

[46] B. D. Cullity, *Introduction to Magnetic Materials* (Addison-Wesley, Reading, MA, 1972).

[47] N. C. Wilson, J. Muscat, D. Mkhonto, P. E. Ngoepe, and N. M. Harrison, Phys. Rev. B **71**, 075202 (2005).

[48] K. Jankowski, P. Malinowski, and M. Polasik, J. Phys. B **12**, 345 (1979).

[49] L. M. L. Daku, A. Vargas, A. Hauser, A. Fouqueau, and M. E. Casida, ChemPhysChem **6**, 1393 (2005).

[50] A. Fouqueau, M. E. Casida, L. M. L. Daku, A. Hauser, and F. Neese, J. Chem. Phys. **122**, 044110 (2005).

[51] A. Fouqueau, S. Mer, M. E. Casida, L. M. L. Daku, A. Hauser, and F. Neese, J. Chem. Phys. **120**, 9473 (2004).

[52] P. Gütlich and H. A. Goodwin, in *Topics in Current Chemistry*, edited by P. Gütlich and H. A. Goodwin, Spin Crossover in Transition Metal Compounds I Vol. 233 (Springer-Verlag, Heidelberg, 2004), p. 1.